Secreted antigen A peptidoglycan hydrolase is essential for *Enterococcus faecium* cell separation and priming of immune checkpoint inhibitor cancer therapy

Steven L. Klupt[1,4], Kyong Tkhe Fam[1,4], Xing Zhang[1,4], Pavan Kumar Chodisetti[1], Abeera Mehmood[1], Tumara Boyd[3], Danielle Grotjahn[3], Donghyun Park[3], Howard C. Hang[1,2*]

[1] Department of Immunology and Microbiology, Scripps Research, La Jolla, California 92037, United States.

[2] Department of Chemistry, Scripps Research, La Jolla, California 92037, United States.

[3] Department of Integrative Structural & Computational Biology, Scripps Research, La Jolla, California 92037, United States.

[4] Contributed equally.

*Correspondence: hhang@scripps.edu

Abstract

Enterococcus faecium is a microbiota species in humans that can modulate host immunity[1], but has also acquired antibiotic resistance and is a major cause of hospital-associated infections[2]. Notably, diverse strains of *E. faecium* produce SagA, a highly conserved peptidoglycan hydrolase that is sufficient to promote intestinal immunity[3-5] and immune checkpoint inhibitor antitumor activity[6]. However, the essential functions of SagA in *E. faecium* were unknown. Here we report that deletion of *sagA* impaired *E. faecium* growth and resulted in bulged and clustered enterococci due to defective peptidoglycan cleavage and cell separation. Moreover, Δ*sagA* showed increased antibiotic sensitivity, yielded lower levels of active muropeptides, displayed reduced activation of the peptidoglycan pattern-recognition receptor NOD2, and failed to promote cancer immunotherapy. Importantly, plasmid-based expression of SagA, but not its catalytically-inactive mutant, restored Δ*sagA* growth, production of active muropeptides and NOD2 activation. SagA is therefore essential for *E. faecium* growth, stress resistance and activation of host immunity.

Main Text

Enterococcus is a genus of Gram-positive bacteria that is composed of more than seventy different species found in diverse environments, both free-living and in relationships with various animals[7]. *Enterococcus faecium* strains have been isolated from humans and reported to have both beneficial and pathogenic properties[2]. Notably, antibiotic resistant strains of *E. faecium*, particularly vancomycin-resistant *E. faecium* (VREfm), have emerged as major causes of healthcare-associated infections[2,8,9], and have been correlated with graft-versus-host disease (GVHD) and increased mortality in allogeneic hematopoietic cell transplantation patients[10]. *E. faecium* has also been recovered from ulcerative colitis and Crohn's disease patients and has been shown to exacerbate intestinal inflammation and colitis in mouse models of inflammatory bowel disease (IBD)[11,12]. However, commensal strains of *E. faecium* have also been reported to enhance intestinal immunity in animal models and have been developed as probiotics[13]. Furthermore, microbiota analysis has shown that *E. faecium* was enriched in immune checkpoint inhibitor (ICI)[14-16] and chimeric antigen receptor (CAR) T-cell therapy-responsive patients[17]. These studies highlight the potential pathogenic and beneficial features of *E. faecium.*

Our laboratory previously investigated the beneficial effects of *E. faecium* on host physiology. We demonstrated that secreted antigen A (SagA), a highly conserved NlpC/P60 peptidoglycan hydrolase in *E. faecium*, was sufficient to confer protection against enteric infections in both *Caenorhabditis elegans* and mice[3]. In mice, *E. faecium* and an *E. faecalis* strain engineered to express SagA both up-regulated expression of mucins and antimicrobial peptides, resulting in improved intestinal barrier function as well as tolerance to *Salmonella enterica* serovar Typhimurium and *Clostridioides difficile* pathogenesis[4,5]. In contrast, wild-type *E. faecalis*, which does not express SagA, did not exhibit these effects. We then determined the X-ray crystal structure of the SagA NlpC/P60 hydrolase domain, and demonstrated that this hydrolase preferentially cleaves crosslinked peptidoglycan fragments into smaller muropeptides (such as GlcNAc-MDP), which more effectively activate the peptidoglycan pattern recognition receptor NOD2 (nucleotide-binding oligomerization domain-containing protein 2) in mammalian cells[5]. Importantly, NOD2 was shown to be required for *E. faecium* stimulation of intestinal immunity and tolerance to infection *in vivo*[4,5]. Moreover, *E. faecium* and SagA were sufficient to protect mice against dextran sodium sulfate-induced colitis that required the expression of NOD2 in myeloid cells[18].

The discovery of *E. faecium* among the microbiota of cancer immunotherapy-responsive patients then motivated our analysis of *Enterococcus* species and SagA in mouse tumor models. Indeed, diverse strains of *E. faecium* that express SagA, but none of the non-SagA-expressing *E. faecalis* strains evaluated, were sufficient to promote ICI (anti-PD-L1, anti-PD-1, anti-CTLA-4) anti-tumor activity against different cancer types in mouse models[6]. Furthermore, other *Enterococcus* species including *E. durans*, *E. hirae* and *E. mundtii,* which each have SagA

orthologs with greater than 80% protein similarity to that of *E. faecium*, were sufficient to enhance anti-PD-L1 antitumor activity[6]. The SagA orthologs from these other *Enterococcus* species were expressed and secreted at similar levels to *E. faecium* SagA and showed similar peptidoglycan hydrolase activity *in vitro*[6]. Importantly, heterologous expression of SagA in inactive bacterial species (*E. faecalis* and *Lactococcus lactis*) was sufficient to promote anti-PD-L1 antitumor activity and required NOD2 *in vivo*[6]. Collectively, these studies demonstrated that *Enterococcus* peptidoglycan remodeling by SagA is sufficient to enhance intestinal immunity against infection and promote cancer immunotherapy. However, the endogenous functions of SagA in *E. faecium* microbiology and modulation of host immunity were not investigated previously, as *sagA* was believed to be an essential gene in *E. faecium* (strain TX1330), as reported by Murray and coworkers[19]. Nevertheless, our collaborative studies with the Duerkop laboratory have indicated that phage-resistant strains of *E. faecium* (strain Com12) containing catalytically inactivating point mutations in *sagA* were still viable[20], suggesting that SagA may not be essential and could be functionally evaluated in *E. faecium.*

Here we report the generation of a Δ*sagA* strain of *E. faecium* (Com15). This strain, generated using RecT-mediated recombineering methods developed by our laboratory[21], exhibited significantly impaired growth (**Fig. 1a**) and sedimentation in liquid culture (**Extended Data Fig. 1b**). Differential interference contrast (DIC) microscopy revealed that Δ*sagA* cells form irregular clusters, as opposed to the typical wild-type morphology of diplococci or short chains (**Fig. 1b**). This cell morphology suggested that dividing Δ*sagA* cells may be unable to separate from one another during binary fission. Indeed, transmission electron microscopy (TEM) of chemically fixed samples confirmed that Δ*sagA* cells have defects in cell separation (**Fig. 1c**). Division septa could form and mature in these cells; however, daughter cells failed to separate, resulting in clusters of unseparated cells. Cells on the periphery of these clusters were highly strained, and in some cases appeared to lyse and leave behind strands of undegraded peptidoglycan. We then performed whole-genome sequencing to assess the fidelity of the Δ*sagA* strain's genome to that of wild-type. While Δ*sagA* contained a small number of mutations, most were outside of open-reading frames (ORFs) or were in genes that are unrelated to peptidoglycan metabolism (**Extended Data Table 1**). One notable mutation, however, was in the predicted glycosidase EFWG_00994. This mutation, L200F, alters a leucine residue that is conserved among GH73 family members and the other putative Com15 glucosaminidases (**Extended Data Table 1**). To confirm that the Δ*sagA* growth defect was truly SagA-dependent and was not an outcome of suppressor mutations, we generated a complementation strain (Δ*sagA*/ p*sagA*) that contained a plasmid expressing *sagA* under control of its native promoter. Western blot analysis with α-SagA polyclonal serum confirmed the deletion and complementation of SagA (**Fig. 1d**). The complementation largely restored the log-phase growth rate and stationary-phase OD of the Δ*sagA* strain to those of wild-type (**Fig. 1a**). It also reversed the liquid-culture sedimentation phenotype (**Extended Data Fig. 1b**) and reduced the cell clustering (**Fig. 1b**) and defective septal separation (**Fig. 1c**).

To investigate the significance of peptidoglycan hydrolase activity in SagA, we generated a catalytically inactive point mutant (C431A) in our *sagA* complementation plasmid. Consistent with our previous biochemical results on recombinant SagA NlpC/P60 domain activity[5,22], the C431A mutant was unable to complement the *sagA* deletion (**Fig. 1a-c**), despite Western blot analysis confirming that the mutant SagA was expressed and secreted properly (**Fig. 1d**). Together, these results demonstrated that catalytically active SagA is required for proper *E. faecium* growth.

Based on the growth defect of Δ*sagA* and the previously-reported antibiotic sensitization effect of catalytically inactivating point mutants in the SagA of *E. faecium* strain Com12[20], we chose to investigate the impact of the *sagA* deletion on the effectiveness of various cell wall-acting antibiotics. Using minimum inhibitory concentration (MIC) test strips of common antibiotics (vancomycin, linezolid, daptomycin, tigecycline, telavancin, fosfomycin, ampicillin, ceftriaxone, and imipenem), we observed increased sensitivity to the β-lactams (ampicillin, ceftriaxone and

imipenem), moderately increased sensitivity to daptomycin, tigecycline, fosfomycin, and linezolid and no change in sensitivity to telavancin and vancomycin (**Extended Data Fig. 2a**). MIC analysis of ampicillin in liquid culture, further demonstrated that Δ*sagA* has increased susceptibility to β-lactam antibiotics, which was abrogated with p*sagA* expression (**Extended Data Fig. 2b**).

To further investigate the growth defect and increased β-lactam antibiotic sensitivity of Δ*sagA*, we performed cryo-electron tomography (cryo-ET) on frozen-hydrated samples to quantify factors such as peptidoglycan thickness, septum thickness, and placement of divisome components at a higher resolution (**Extended Data Fig. 3a,b**). There was no statistically significant change in peptidoglycan thickness and septum thickness in Δ*sagA* and Δ*sagA/* p*sagA* cells compared to wild-type cells (**Extended Data Fig 3c,d**). Similar to previous studies of *Bacillus subtilis*[23], the divisome machinery was directly observable as concentric rings in cross-sectional images generated by cryo-ET in *E. faecium* (**Extended Data Fig. 4a-d**). We quantified the distances from these rings in order to assess potential differences in divisome placement (**Extended Data Fig. 4e**). The distance between the septal membrane and the distal ring of the divisome showed a slight increase, but we did not observe any statistical difference between the distance from the septal membrane to the proximal ring and the ratio between the proximal and distal rings in wild-type, Δ*sagA*, and complementation (**Extended Data Fig. 3e**, **Extended data Fig. 4f,g**). However, we observed that the placement and projection angle of growing septa were significantly altered in Δs*agA* but were mostly restored by complementation (**Fig. 2a-f**). Both room temperature TEM and cryo-ET revealed that *sagA* complementation largely restored the wild-type cell morphology of Δ*sagA* to that of wild-type (**Fig. 2, Extended Data Fig. 3 and 4**). The complemented cells separate from one another and mostly take the form of diplococci. These results suggest that the ultrastructure of the peptidoglycan cell wall is unchanged as a result of *sagA* deletion, but peptidoglycan cleavage, divisome angle and septal resolution are impaired.

We then investigated Δ*sagA* peptidoglycan composition and activation of NOD2 immune signaling. To evaluate peptidoglycan composition, *E. faecium* sacculi were isolated, subjected to mutanolysin digestion, analyzed by liquid chromatography mass spectrometry (**Extended Data Fig. 5**) and quantified (**Fig. 3a,b**), as previously described[5]. The Δ*sagA* strain showed decreased levels of small muropeptides (peaks 2, 3 and 7) compared to *E. faecium* Com15, which was restored in Δ*sagA*/ p*sagA* (**Fig. 3a**). Moreover, we observed increased amounts of crosslinked peptidoglycan fragments (peaks 13 and 14) (**Fig. 3a**). Notably, GlcNAc-MDP, which we previously demonstrated more effectively activates NOD2[5], was significantly decreased in Δ*sagA* (**Fig. 3b**). Indeed, our analysis using HEK-Blue™ NF-κB reporter cells demonstrated that Δ*sagA* exhibits significantly decreased NOD2 activation compared to *E. faecium* Com15. This activation was restored in Δ*sagA*/ p*sagA* (**Fig. 3c**). For these assays, we used comparable numbers of bacteria to account for defects in Δ*sagA* growth, which was confirmed by colony-forming unit analysis of bacteria per well (**Fig. 3d**). These results were consistent with our *in vitro* analysis of recombinant SagA with purified peptidoglycan fragments, which showed the generation of small muropeptides (GlcNAc-MDP) that more potently activated NOD2 compared to crosslinked muropeptides[5], and demonstrated that SagA is essential for *E. faecium* immune activation *ex vivo*.

We next investigated if SagA is crucial for *E. faecium* colonization and immune modulation *in vivo* using well-established mouse models of ICI cancer immunotherapy (**Fig. 4a**). We had previously demonstrated that heterologous expression of SagA was sufficient to promote *E. faecalis* and *L. lactis* ICI antitumor activity and required *Nod2* expression in mice[6]. However, activity of wild-type *E. faecium* in *Nod2*$^{-/-}$ mice was not determined. Indeed, oral administration of *E. faecium* to microbiota-depleted/antibiotic-treated C57BL/6 mice promoted anti-PD-1 antitumor activity against MC-38 tumor growth in *Nod2*$^{+/-}$, but failed to do so in *Nod2*$^{-/-}$ mice (**Fig. 4b**). To determine if SagA is required for *E. faecium* function *in vivo*, antibiotic-treated mice were colonized with *E. faecium* Com15 or Δ*sagA*. Notably, the antitumor activity of *E. faecium* was abolished in Δ*sagA* strain (**Fig. 4c**) even though both bacterial strains colonized mice at comparable levels, as judged by fecal *E. faecium* levels (**Fig. 4d**). We then performed immune

profiling of tumor infiltrating lymphocytes (TILs) using flow cytometry (**Extended Data Fig. 6**). Compared to *E. faecium* Com15 colonized mice, Δ*sagA* colonized mice showed no difference in the total amount of the tumor infiltrating $CD45^+$ cells (**Fig. 4e**) or $CD4^+$ $FoxP3^+$ regulatory T cells (**Fig 4f**), but resulted in fewer $CD3^+$ $CD8^+$ T cells (**Fig. 4g**). Furthermore, $granzymeB^+$ $CD8^+$ T cells, $Ki67^+$ $CD8^+$ T cells and $PD\text{-}1^+$ $CD8^+$ T cells levels were also lower in Δ*sagA* colonized mice (**Fig 4h-j**). We evaluated the activity Δ*sagA*/ p*sagA* strain in these experiments (data not shown), but the results were inconclusive likely due to instability of p*sagA* plasmid in *E. faecium in vivo*. Collectively, these results demonstrate SagA is not essential for *E. faecium* colonization, but required for promoting the ICI antitumor activity *in vivo*.

E. faecium is a prominent microbiota species and pathogen in animals and humans. While *E. faecium* identification and dominance in fecal microbiota have been correlated with health and disease outcomes, the underlying mechanisms have only begun to emerge. Our previous gain-of-function studies with recombinant protein and engineered bacterial strains demonstrated that SagA, a unique secreted peptidoglycan hydrolase that is highly conserved in *E. faecium* strains and other *Enterococcus* species, but not *E. faecalis*, is sufficient to activate NOD2 and promote host immunity *in vivo*[3-6]. However, the endogenous functions of SagA in *E. faecium* were unknown. Based on the results described above, we now show that SagA peptidoglycan hydrolase activity is not required for *E. faecium* viability, but essential for proper growth and specifically for septal separation following cell division (**Fig. 1 and 2**). These results are consistent with key peptidoglycan hydrolases in other bacterial species, such as AmiA/B in *Escherichia coli*[24], CwlO/LytE in *Bacillus subtilis*[25,26], PcsB in *Streptococcus pneumoniae*[27] and RipC in *Mycobacterium tuberculosis*[28]. Although the mechanisms of regulation may differ amongst peptidoglycan hydrolases and remain to be determined for SagA, the *sagA* promoter contains sequence motifs that may be regulated by WalRK two-component systems[29] and the SagA protein contains a N-terminal coil-coil domain that may interact with *E. faecium* divisome components, which warrants further investigation in the future. Notably, the deletion of *sagA* in *E. faecium* Com15 also renders this strain more susceptible to cell wall-acting antibiotics (**Extended Data Fig. 2**), akin to inactive SagA variants in *E. faecium* Com12[20], suggesting SagA and its related peptidoglycan hydrolases may be potential antibacterial targets to use in combination with existing antibiotics. Interestingly, clade B strains of *E. faecium* including Com12 and Com15 have been suggested to be reclassified as *Enterococcus lactis* based on genomic and phenotypic similarity[30,31]. Nonetheless, SagA orthologs have greater than 90 percent protein sequence identity within the C-terminal NlpC/P60 hydrolase domain of ICI therapy-promoting *Enterococcus* species (*E. faecium-clade A and B, E. durans, E. hirae* and *E. mundtii*)[6]. Notably, all the *Enterococcus* strains and species that express active SagA orthologs that we have analyzed promote ICI cancer immunotherapy in mouse models[6].

Beyond intrinsic functions in *E. faecium* microbiology, we have also demonstrated for the first time that SagA is essential for the activation of host immunity. Notably, we showed that Δ*sagA* does not generate significant amounts of non-crosslinked muropeptides (i.e. GlcNAc-MDP) that are sensed by the peptidoglycan pattern recognition receptor NOD2 (**Fig. 3**). Indeed, Δ*sagA* failed to activate NOD2 *ex vivo* (**Fig. 3**) and promote ICI antitumor activity in mouse models compared to wild-type *E. faecium* (**Fig. 4**). Collectively, our results provide important mechanistic insight on SagA in peptidoglycan remodeling for bacterial cell separation and reveal an essential feature of *E. faecium* (**Extended Data Fig. 7**) and other related *Enterococcus* species that are associated human health, disease, and response to therapy.

Methods

Bacterial growth

All cultures of *E. faecium* (**Extended Data Table 2**) and *E. coli* were grown in a shaking incubator at 37°C and 220 RPM with relevant antibiotics. *E. faecium* was grown in Brain Heart Infusion (BHI) broth or on BHI agar supplemented as needed with 10 µg/mL chloramphenicol or 50 µg/mL erythromycin. *E. coli* was grown in Luria-Bertani (LB) broth or on LB agar supplemented as needed with 10 ug/mL chloramphenicol or 150 ug/mL erythromycin. Growth curve experiments were performed in 96-well plate format using a BioTek (Agilent) plate reader set to 37°C continuous shaking. Starter cultures were grown overnight shaking at 37°C in BHI with appropriate antibiotics. For the growth curves, the starter cultures were diluted to an OD of 0.01 in fresh BHI in a sterile 96-well plate.

sagA knockout generation

The Δ*sagA::cat* knockout was generated following methods previously described by our laboratory [20]. Briefly, double stranded DNA (dsDNA) templates were assembled by cloning *sagA* homology arms flanking a chloramphenicol acetyl transferase (*cat*) antibiotic marker into pET21, and amplified by PCR. PCR was performed using Q5 high-fidelity DNA polymerase (New England BioLabs) according to the manufacturer's instructions. The dsDNA was electroporated into electrocompetent *E. faeicum* Com15 cells harboring RecT (prepared using the lysozyme method previously described in [Victor's paper]). The transformants were verified by colony PCR.

sagA complementation and mutagenesis

sagA complementation was accomplished using a pAM401-based plasmid containing *sagA* under the control of its native promoter. Primers used to make the p*sagA* plasmids and empty vector are reported in **Extended Data Tables 4-5**. Plasmids were transformed by electroporation into electrocompetent Δ*sagA* cells.

Western blot analysis

Cultures were grown overnight shaking at 37°C with appropriate antibiotics. The next day, the cultures were centrifuged and the pellets were separated from the supernatants. The pellets were resuspended in lysis buffer (50 mM Bis-Tris pH 7.5, 4% SDS, 0.1 mg/mL lysozyme, 25 U benzonaze), and then lysed by bead beating (FastPrep system, MP Biomedicals). Proteins were precipitated from the supernatants by methanol-chloroform precipitation and resuspended in water. Proteins from the pellets and supernatants were quantified by BCA analysis (ThermoFischer), run on a Stain-Free gel (BioRad), and imaged. Protein bands were then transferred to a nitrocellulose membrane by semi-dry transfer. The membrane was blocked for 1 hour with TBST+5% powdered milk at room temperature, then stained with primary antibody (rabbit anti-SagA polyclonal sera) diluted 1:50,000 in TBST+5% milk for 1 hour at room temperature. The membrane was then stained with secondary antibody (goat anti-rabbit antibody, HRP-conjugate) diluted 1:20,000 in TBST+5% powdered milk.

Transmission electron microscopy

Cultures were grown overnight shaking at 37°C in BHI with appropriate antibiotics. Bacteria were then rinsed with 0.1M cacodylate buffer followed by immersion in oxygenated 2.5% glutaraldehyde and 4% paraformaldhyde fixative in 0.1M sodium cacodylate buffer (pH 7.1) and embedded in low-melting point agar then fixed overnight at 4°C. After washing in 0.1M sodium cacodylate buffer, the samples were post-fixed in buffered 1% osmium tetroxide plus 1.5% potassium ferrocyanide for 1 hour at 4°C, rinsed in ddH_2O and stained *en bloc* with 0.5% uranyl acetate overnight at 4°C. Samples were washed in ddH_2O and dehydrated through a graded ethanol series followed by acetone and infiltrated with LX-112 (Ladd) epoxy resin and polymerized

at 60°C. Thin sections (70-nm) were imaged at 80kV with a ThermoFisher Talos L120C transmission electron microscope and images were acquired with a CETA 16M CMOS camera.

Cryo-electron tomography

E. faecium strains used in the cryo-ET experiments were grown overnight at 37 °C in BHI broth with appropriate antibiotics. Fresh cultures were prepared from a 1:100 dilution of the overnight culture and then grown at 37 °C to late log phase. The culture was centrifuged at 1000 x g for 5 minutes. The pellet was resuspended with BHI broth containing 5% glycerol to OD600 of 3. 5 µl of *ΔsagA* and *ΔsagA*/p*sagA* samples were deposited onto freshly glow-discharged (Pelco easiGlow; 25 seconds glow at 15mA) Quantifoil R2/1 copper 200 mesh grids for 1 minute, back-side blotted with filter paper (Whatman Grade 1 filter paper), and frozen in liquid ethane using a gravity-driven homemade plunger apparatus (inside a 4° cold room with a ≥ 95% relative humidity). The WT Com15 samples were frozen using a Vitrobot Mark IV (Thermo Fisher Scientific) in liquid ethane/propane mixture. The Vitrobot was set to 22C° at 90% humidity, and manually back-side blotted. The vitrified grids were later clipped with Cryo-FIB autogrids (Thermo Fisher Scientific) prior to milling.

Cryo-FIB milling was performed using Aquilos dual-beam cryo-FIB/SEM instrument (Thermo Fisher Scientific). The vitrified sample was sputtered metallic platinum for 15 seconds, followed by a coating of organometallic platinum for 8-9 seconds to protect the sample, and then the sample was sputtered with metallic platinum for 15 seconds to prevent drifting during milling. Target sites were milled manually with a gallium ion beam to generate lamellae with a thickness of approximately <150 nm. Finally, the lamellae were sputtered with metallic platinum for 3-4 seconds to create bead-like fiducial inclusions that aid in tiltseries alignment.

Lamellae were imaged with a Titan Krios microscope (Thermo Fisher Scientific) equipped with a field emission gun, an energy filter, and a direct-detection device (Gatan K3). An energy filter with a slit width of 20 eV was used for data acquisition. The SerialEM package[32] with PACEtomo scripts[33] was used to collect 39 image stacks at a range of tilt angles between +57° and -57° (3° step size) using a dose-symmetric scheme with a cumulative dose of ~117 $e^{-}/Å^2$. Data was collected with a magnification resulting in 2.64 Å/pixel and a nominal defocus of ~ -5 µm. Image stacks containing 10 to 15 images were motion corrected using Motioncor2[34] and then assembled into drift-corrected stacks using IMOD. The drift-corrected stacks were aligned and reconstructed by IMOD marker-dependent alignment[35]. Representative tomograms and raw tiltseries are publicly available: EMD-42074, EMD-42086, EMD-42087, and EMPIAR-11692.

All the tomograms were denoised with IsoNet[36], a deep learning-based software package. Segmentation was performed using Amira software (Thermo Fisher Scientific). All the renderings were visualized in 3D using UCSF ChimeraX[37].

Antibiotic sensitivity assays

MIC test strip analysis. Overnight cultures were diluted to an OD of 0.2. 200 µL of diluted culture were then spread onto a BHI agar plate using glass beads (for strains containing p*sagA* or empty pAM401E, BHI plates with 50 µg/mL erythromycin were used). Plates were placed in a 37°C incubator for approximately one hour to allow the liquid to soak into the plate. MIC test strips (Liofilchem) were then placed at the center of the agar plates using sterile tweezers. Plates were incubated overnight at 37°C and photographed the next day. For ampicillin liquid culture MIC experiments, the same protocol as the growth curve experiments described above were used, except the cells were treated with various serially-diluted concentrations of ampicillin.

NOD2 activation assays

The assay was followed by manufacturer's protocol. In brief, HEK-Blue™ cells were seeded in 96-well plate at the cell density $6x10^4$ cells/well. *E. faecium* were grown to an OD of ~0.5 from overnight inoculant, washed with PBS and resuspended in Opti-MEM. Live bacteria were given

to HEK-Blue™ at multiplicity of infection (MOI) 1 and incubated for 4 hours at 37°C. After 4 hours, HEK-Blue™ were carefully washed with PBS and the media was replaced with DMEM supplemented with gentamycin (250 µg/mL) to kill extracellular bacteria. Cells were incubated at 37°C for an additional 16 hours. NOD2 activation was measured by detecting NF-κB-inducible secreted embryonic alkaline phosphatase expression in the media using colorimetric QUANTI-Blue™ detection assay. Synthetic NOD2 agonist muramyl dipeptide (MDP) was used as a positive control, fold-change of activation was expressed relative to untreated HEK-Blue™ cells control. For activation by secreted PG fragments, conditioned supernatants were collected from *E. faecium* at early stationary phase. Supernatants were passed through 0.22 µm filters. 5 µL of supernatants were given to HEK-Blue™ cells and incubated at 37°C for 16 hours.

LC-MS analysis of peptidoglycan

Peptidoglycan was extracted from bacteria (wild-type *E. faecium*, Δ*sagA*, and Δ*sagA*/p*sagA*) and digested with mutanolysin from *Streptomyces globisporus* (Sigma, 10 KU/ml of mutanolysin in ddH_2O) as previously described[5]. The resulting soluble muropeptide mixture was treated with sodium borohydride in 0.25 M boric acid (pH 9) for 1 hour at room temperature, quenched with orthophosphoric acid, and pH adjusted to 2-3. Samples were centrifuged at 20,000xg for 10 minutes. Then, the reduced peptidoglycan was analyzed by 1290 Infinity II LC/MSD system (Agilent technologies) using Poroshell 120 EC-C18 column (3 x 150 mm, 2.7 µM). Samples were run at flow rate 0.5 mL/min in mobile phase (A: water, 0.1% formic acid) and an eluent (B: acetonitrile, 0.1% formic acid) using following gradient: 0-5 min: 2% B, 5-65 min: 2-10% B. The absorbance of the eluting peaks was measured at 205 nm. Masses of peaks were detected with MSD API-ES Scan mode (m/z = 200-2500) (**Extended Data Table 6**).

Animals

Specific pathogen-free, seven-week-old male C57BL/6 (B6,000664) mice were obtained from Scripps Rodent Breeding Colony. For breeding, *Nod2*$^{-/-}$ (B6.129S1-*Nod2*^{tm1Flv}/J) and C57BL/6 (B6,000664) mice were obtained from The Jackson Laboratory. *Nod2*$^{+/-}$ and *Nod2*$^{-/-}$ littermate cohorts were generated by in-house breeding. Genotyping was performed according to the protocols established for the respective strains by The Jackson Laboratory (Protocol 25069). Mice were housed in autoclaved caging with SaniChip bedding and enrichment for nest building on a 12 h light/dark cycle. Mice were provided gamma-irradiated chow (LabDiet, 5053) and sterile drinking water ad libitum. Animal care and experiments were conducted in accordance with NIH guidelines and approved by the Institutional Animal Care and Use Committee at Scripps Research (Protocol AUP-21-095).

Tumor challenge, growth and treatment experiments

Seven-week-old mice were pre-treated with antibiotic (5 g L-1 streptomycin, 1 g L-1 colistin sulfate, and 1 g L-1 ampicillin) for one week prior to bacterial colonization, as previously described[6]. *E. faecium* Com15 and *ΔsagA* strains were grown to late logarithmic phase and diluted to OD600=0.46, then diluted 5x with drinking water to (OD 0.46 equal to 10^8 CFU ml^{-1}). Three days after bacterial colonization (Day 0), mice were subcutaneously implanted with B16F10 melanoma cells (10^5 cells per mice) or MC38 tumor cells ($3x10^5$ cells per mice) with Matrigel matrix (Corning, 356231). Once the tumors established (around 100 mm^3), tumor volume was measured every two days by digital calipers and was calculated as length x width^2 x 0.5, where the width was the smaller of the two measurements. For B16F10 implanted mice, 20 ug anti–PD-L1 (BioXCell, BP0101) were administered to the mice at Day 6, 9 and 12 by intraperitoneal injection in 200 µL antibody buffer solution (BioXCell, PH 6.5 dilution buffer). For MC38 implanted mice, 100 ug anti–PD-1 (BioXCell, BP0146) were administered to the mice at Day 5, 7, 9, 11 and 14 by intraperitoneal injection in 200 µL antibody buffer solution (BioXCell, PH 7.0 dilution buffer). Mice

were euthanized with CO2 asphyxiation when the tumors larger than 1.5 cm^3 or any ulceration or lesioning developed.

Fecal colonization analysis

Fecal samples were sterilely collected six days after the start of bacterial administration. Fecal samples were weighed, resuspended in sterile PBS, homogenized by douncing with sterile pestles, serially diluted in sterile PBS, and then plated by drip assay onto selective HiCrome™ *Enterococcus faecium* Agar plates (HIMEDIA 1580) with *Enterococcus faecium* selective supplement (FD226, HIMEDIA). Plates were incubated for 48 h at 37 °C under ambient atmosphere and colonies were manually counted.

Cell isolation and flow cytometry analysis

Tumor dissection and cell isolation were performed as previously described[6]. The dissected tumor samples were placed in RPMI with 1.5 U mL^{-1} Liberase TM (Roche 5401119001), 0.2 mg mL-1 DNase I (Worthington Biochemical LS002006) and ceramic spheres (6.35 mm, MP Biomedicals 116540424-CF) for 30 min at 37 °C with gentle shaking. Samples were then filtered and resuspended in 5 mL of red blood cell lysis buffer (ThermoFisher 00-4333-57) for 5 min at room temperature. Cells were washed and incubate with 1:1000 Zombie Yellow stain (BioLegend 423103) for 20 min at room temperature. After two times wash, samples were incubated with 20 µL of staining buffer containing 0.5 µL of TruStain FcX anti–mouse CD16/32 blocking agent (BioLegend 101319) for 30 min at room temperature. Sample directly incubate with anti-CD4 (BUV496, GK1.5, BD Biosciences 612953) and anti-PD-1 (BV711, CD279, BD Biosciences 135231) for another 30 min on ice. Cells were washed twice, fixed and permeabilized with the FoxP3/Transcription Factor Staining Buffer Set (ThermoFisher 00-5523-00) overnight at 4°C. Cells were washed twice with perm buffer and then incubated with 20 µL of perm buffer containing 10% rat serum (ThermoFisher 24-5555-94) for 20 min on ice. Cells were then stainied with the follow antibodies for 20 min on ice: anti-CD45 (APC-Fire 750, 30-F11, BioLegend 103153), anti-CD3 (BV785, 17A2, BioLegend 100232), anti-NK1.1 (BV480, PK136, BD Biosciences 746265) anti-CD8 (PE-Cy-7, 53-6.7, BioLegend 100721), anti-FoxP3 (AF532, FJK-16s, ThermoFisher 58-5773-80), anti-Granzyme B (PE-CF594, GB11, BD Biosciences 562462) and anti-Ki67 (FITC, SolA15, LifeTech 11-5698-82). Samples were analyzed using Cytek Aurora spectral flow cytometer and the data were analyzed using FlowJo Version 10.9.0.

Acknowledgements

This project was funded by the National Institutes of Health R01 CA245292 grant to H.C.H and Scripps Research start-up funds to H.C.H and D.P. A.M. is supported by David C. Fairchild Endowed Fellowship to the Skaggs Graduate Program at Scripps Research. We thank Victor Chen for guidance on RecT-mediated recombineering in *E. faecium*. We thank Scott Henderson, Kimberly Vanderpool and Theresa Fassel for assistance and transmission electron microscopy analysis in the Scripps Microscopy Core.

Author information

Authors and Affiliations

Department of Immunology and Microbiology, Scripps Research, La Jolla, California 92037, United States. Steven L. Klupt, Kyong Tkhe Fam, Xing Zhang, Pavan Kumar Chodisetti, Abeera Mehmood, Howard C. Hang

Department of Chemistry, Scripps Research, La Jolla, California 92037, United States. Howard C. Hang

Department of Integrative Structural & Computational Biology, Scripps Research, La Jolla, California 92037, United States. Tumara Boyd, Danielle Grotjahn, Donghyun Park

Contributions

S.L.K and H.C.H conceived the project. S.L.K and P.C.K performed microbiology studies. K.F. performed LC-MS analysis of peptidoglycan and NOD2 activation assays**.** X.Z. and A.M. performed immune checkpoint inhibitor antitumor and flow cytometry studies. T.B. and D.P. performed cryo-electron tomography analysis. D.G. established Scripps Research cryo-ET facility, provided training and technical assistance. S.L.K and H.C.H wrote the manuscript, which was edited by all the other authors and revised the manuscript.

Corresponding author

Howard C. Hang

Ethics declarations

H.C.H. has filed patent applications (PCT/US2016/028836, PCT/US2020/019038) for the commercial use of SagA-bacteria to improve intestinal immunity and checkpoint blockade immunotherapy, which has been licensed by Rise Therapeutics for probiotic development.

Extended data

References

1 Griffin, M. E. & Hang, H. C. Microbial mechanisms to improve immune checkpoint blockade responsiveness. *Neoplasia* **31**, 100818, doi:10.1016/j.neo.2022.100818 (2022).

2 Van Tyne, D. & Gilmore, M. S. Friend turned foe: evolution of enterococcal virulence and antibiotic resistance. *Annu Rev Microbiol* **68**, 337-356, doi:10.1146/annurev-micro-091213-113003 (2014).

3 Rangan, K. J. *et al.* A secreted bacterial peptidoglycan hydrolase enhances tolerance to enteric pathogens. *Science* **353**, 1434-1437, doi:10.1126/science.aaf3552 (2016).

4 Pedicord, V. A. *et al.* Exploiting a host-commensal interaction to promote intestinal barrier function and enteric pathogen tolerance. *Sci Immunol* **1**, doi:10.1126/sciimmunol.aai7732 (2016).

5 Kim, B. *et al.* Enterococcus faecium secreted antigen A generates muropeptides to enhance host immunity and limit bacterial pathogenesis. *Elife* **8**, doi:10.7554/eLife.45343 (2019).

6 Griffin, M. E. *et al.* Enterococcus peptidoglycan remodeling promotes checkpoint inhibitor cancer immunotherapy. *Science* **373**, 1040-1046, doi:10.1126/science.abc9113 (2021).

7 Lebreton, F. *et al.* Tracing the Enterococci from Paleozoic Origins to the Hospital. *Cell* **169**, 849-861 e813, doi:10.1016/j.cell.2017.04.027 (2017).

8 Fiore, E., Van Tyne, D. & Gilmore, M. S. Pathogenicity of Enterococci. *Microbiol Spectr* **7**, doi:10.1128/microbiolspec.GPP3-0053-2018 (2019).

9 Garcia-Solache, M. & Rice, L. B. The Enterococcus: a Model of Adaptability to Its Environment. *Clin Microbiol Rev* **32**, doi:10.1128/CMR.00058-18 (2019).

10 Stein-Thoeringer, C. K. *et al.* Lactose drives Enterococcus expansion to promote graft-versus-host disease. *Science* **366**, 1143-1149, doi:10.1126/science.aax3760 (2019).

11 Barnett, M. P. *et al.* Changes in colon gene expression associated with increased colon inflammation in interleukin-10 gene-deficient mice inoculated with Enterococcus species. *BMC Immunol* **11**, 39, doi:10.1186/1471-2172-11-39 (2010).

12 Seishima, J. *et al.* Gut-derived Enterococcus faecium from ulcerative colitis patients promotes colitis in a genetically susceptible mouse host. *Genome Biol* **20**, 252, doi:10.1186/s13059-019-1879-9 (2019).

13 Hanchi, H., Mottawea, W., Sebei, K. & Hammami, R. The Genus Enterococcus: Between Probiotic Potential and Safety Concerns-An Update. *Front Microbiol* **9**, 1791, doi:10.3389/fmicb.2018.01791 (2018).

14 Gopalakrishnan, V. *et al.* Gut microbiome modulates response to anti-PD-1 immunotherapy in melanoma patients. *Science* **359**, 97-103, doi:10.1126/science.aan4236 (2018).

15 Routy, B. *et al.* Gut microbiome influences efficacy of PD-1-based immunotherapy against epithelial tumors. *Science* **359**, 91-97, doi:10.1126/science.aan3706 (2018).

16 Matson, V. *et al.* The commensal microbiome is associated with anti-PD-1 efficacy in metastatic melanoma patients. *Science* **359**, 104-108, doi:10.1126/science.aao3290 (2018).

17 Smith, M. *et al.* Gut microbiome correlates of response and toxicity following anti-CD19 CAR T cell therapy. *Nat Med* **28**, 713-723, doi:10.1038/s41591-022-01702-9 (2022).
18 Jang, K. K. *et al.* Antimicrobial overproduction sustains intestinal inflammation by inhibiting Enterococcus colonization. *Cell Host Microbe*, doi:10.1016/j.chom.2023.08.002 (2023).
19 Teng, F., Kawalec, M., Weinstock, G. M., Hryniewicz, W. & Murray, B. E. An Enterococcus faecium secreted antigen, SagA, exhibits broad-spectrum binding to extracellular matrix proteins and appears essential for E. faecium growth. *Infect Immun* **71**, 5033-5041, doi:10.1128/IAI.71.9.5033-5041.2003 (2003).
20 Canfield, G. S. *et al.* Lytic bacteriophages facilitate antibiotic sensitization of Enterococcus faecium. *Antimicrob Agents Chemother*, doi:10.1128/AAC.00143-21 (2021).
21 Chen, V., Griffin, M. E., Maguin, P., Varble, A. & Hang, H. C. RecT Recombinase Expression Enables Efficient Gene Editing in Enterococcus spp. *Appl Environ Microbiol* **87**, e0084421, doi:10.1128/AEM.00844-21 (2021).
22 Espinosa, J. *et al.* Enterococcus NlpC/p60 Peptidoglycan Hydrolase SagA Localizes to Sites of Cell Division and Requires Only a Catalytic Dyad for Protease Activity. *Biochemistry* **59**, 4470-4480, doi:10.1021/acs.biochem.0c00755 (2020).
23 Khanna, K., Lopez-Garrido, J., Sugie, J., Pogliano, K. & Villa, E. Asymmetric localization of the cell division machinery during Bacillus subtilis sporulation. *Elife* **10**, doi:10.7554/eLife.62204 (2021).
24 Yang, D. C. *et al.* An ATP-binding cassette transporter-like complex governs cell-wall hydrolysis at the bacterial cytokinetic ring. *Proc Natl Acad Sci U S A* **108**, E1052-1060, doi:10.1073/pnas.1107780108 (2011).
25 Meisner, J. *et al.* FtsEX is required for CwlO peptidoglycan hydrolase activity during cell wall elongation in Bacillus subtilis. *Mol Microbiol* **89**, 1069-1083, doi:10.1111/mmi.12330 (2013).
26 Wilson, S. A., Tank, R. K. J., Hobbs, J. K., Foster, S. J. & Garner, E. C. An exhaustive multiple knockout approach to understanding cell wall hydrolase function in Bacillus subtilis. *mBio*, e0176023, doi:10.1128/mbio.01760-23 (2023).
27 Sham, L. T., Barendt, S. M., Kopecky, K. E. & Winkler, M. E. Essential PcsB putative peptidoglycan hydrolase interacts with the essential FtsXSpn cell division protein in Streptococcus pneumoniae D39. *Proc Natl Acad Sci U S A* **108**, E1061-1069, doi:10.1073/pnas.1108323108 (2011).
28 Mavrici, D. *et al.* Mycobacterium tuberculosis FtsX extracellular domain activates the peptidoglycan hydrolase, RipC. *Proc Natl Acad Sci U S A* **111**, 8037-8042, doi:10.1073/pnas.1321812111 (2014).
29 Brogan, A. P. & Rudner, D. Z. Regulation of peptidoglycan hydrolases: localization, abundance, and activity. *Curr Opin Microbiol* **72**, 102279, doi:10.1016/j.mib.2023.102279 (2023).
30 Belloso Daza, M. V. *et al.* Distinction between Enterococcus faecium and Enterococcus lactis by a gluP PCR-Based Assay for Accurate Identification and Diagnostics. *Microbiol Spectr* **10**, e0326822, doi:10.1128/spectrum.03268-22 (2022).

31 Belloso Daza, M. V., Cortimiglia, C., Bassi, D. & Cocconcelli, P. S. Genome-based studies indicate that the Enterococcus faecium Clade B strains belong to Enterococcus lactis species and lack of the hospital infection associated markers. *Int J Syst Evol Microbiol* **71**, doi:10.1099/ijsem.0.004948 (2021).

32 Mastronarde, D. N. Automated electron microscope tomography using robust prediction of specimen movements. *J Struct Biol* **152**, 36-51, doi:10.1016/j.jsb.2005.07.007 (2005).

33 Eisenstein, F. *et al.* Parallel cryo electron tomography on in situ lamellae. *Nat Methods* **20**, 131-138, doi:10.1038/s41592-022-01690-1 (2023).

34 Zheng, S. Q. *et al.* MotionCor2: anisotropic correction of beam-induced motion for improved cryo-electron microscopy. *Nat Methods* **14**, 331-332, doi:10.1038/nmeth.4193 (2017).

35 Mastronarde, D. N. & Held, S. R. Automated tilt series alignment and tomographic reconstruction in IMOD. *J Struct Biol* **197**, 102-113, doi:10.1016/j.jsb.2016.07.011 (2017).

36 Liu, Y. T. *et al.* Isotropic reconstruction for electron tomography with deep learning. *Nat Commun* **13**, 6482, doi:10.1038/s41467-022-33957-8 (2022).

37 Goddard, T. D. *et al.* UCSF ChimeraX: Meeting modern challenges in visualization and analysis. *Protein Sci* **27**, 14-25, doi:10.1002/pro.3235 (2018).

Figures and Captions

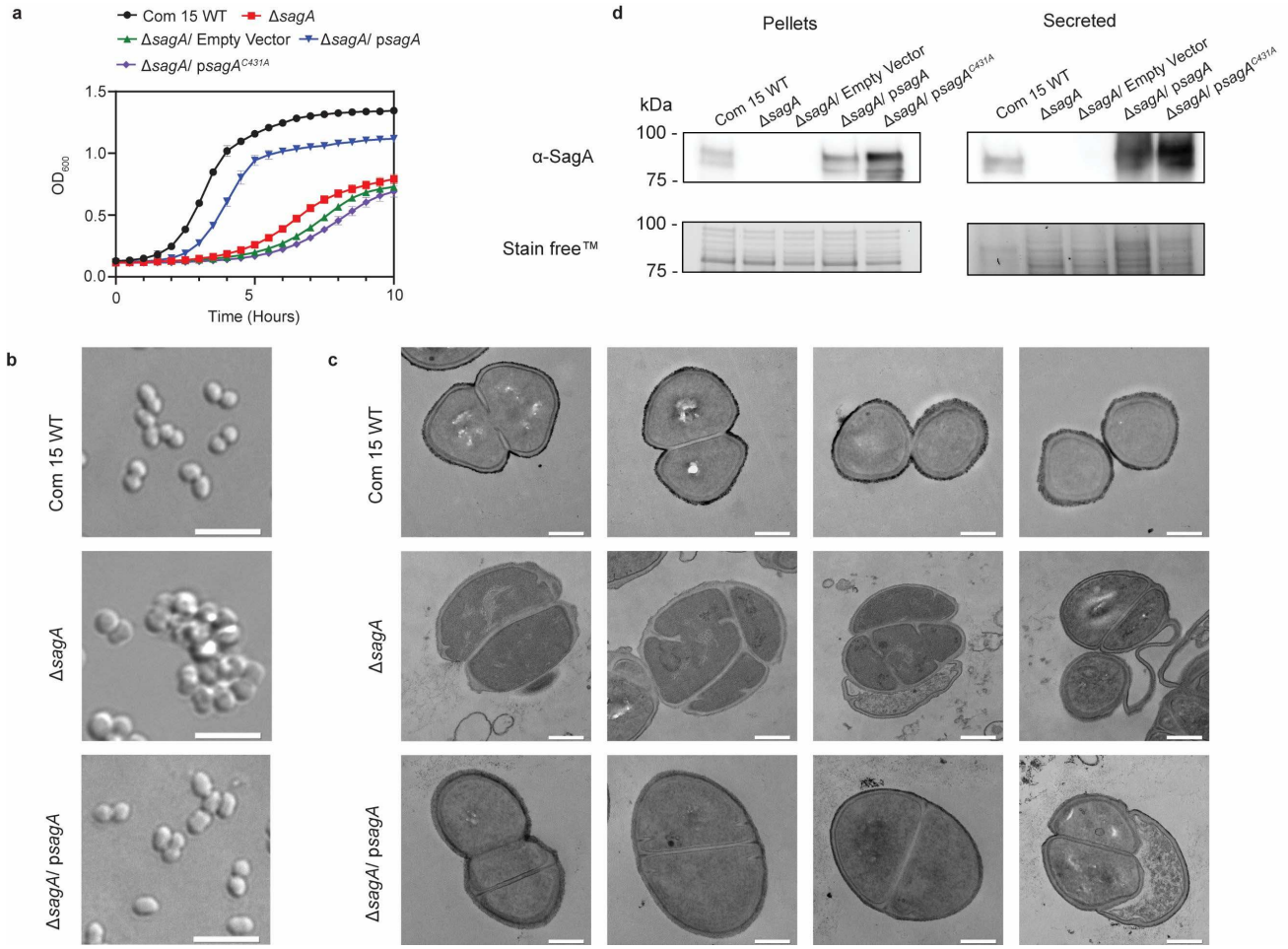

Figure 1. Growth and morphology phenotypes of wild type, *ΔsagA* and p*sagA* complemented *E. faecium* Com15 strains. a, Growth curves of *E. faecium* WT Com15, Δ*sagA*, and complementation strains with functional and nonfunctional *sagA* genes. **b**, DIC microscopy of wild-type E. faecium, *ΔsagA* and *ΔsagA/* p*sagA* complemented strains. Scale bar = 5 μm. **c**, Transmission electron microscopy (TEM) of *E. faecium* WT Com15, *ΔsagA*, and *ΔsagA/* p*sagA* complemented strains. Scale bar = 0.2 μm. **d**, α-SagA Western Blot of *E. faecium* WT Com15, Δ*sagA*, and complementation strains with functional and nonfunctional *sagA* genes, on both whole cell lysate (pellets) and total secreted proteins (secreted).

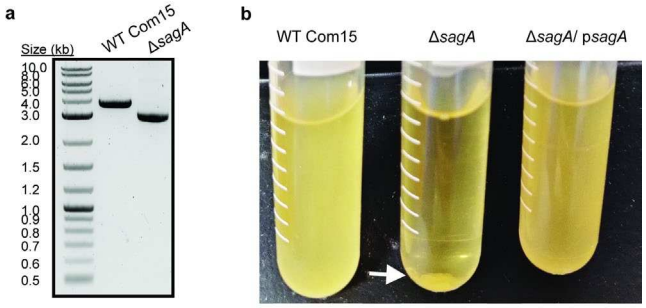

Extended Data Figure 1. Analysis of *E. faecium* Δ*sagA* deletion and complementation studies. a, PCR validation of Δ*sagA* deletion. **b**, Δ*sagA* cells are sedimented at the bottom of the tube compared to *E. faecium* WT Com15 and Δ*sagA* / p*sagA*.

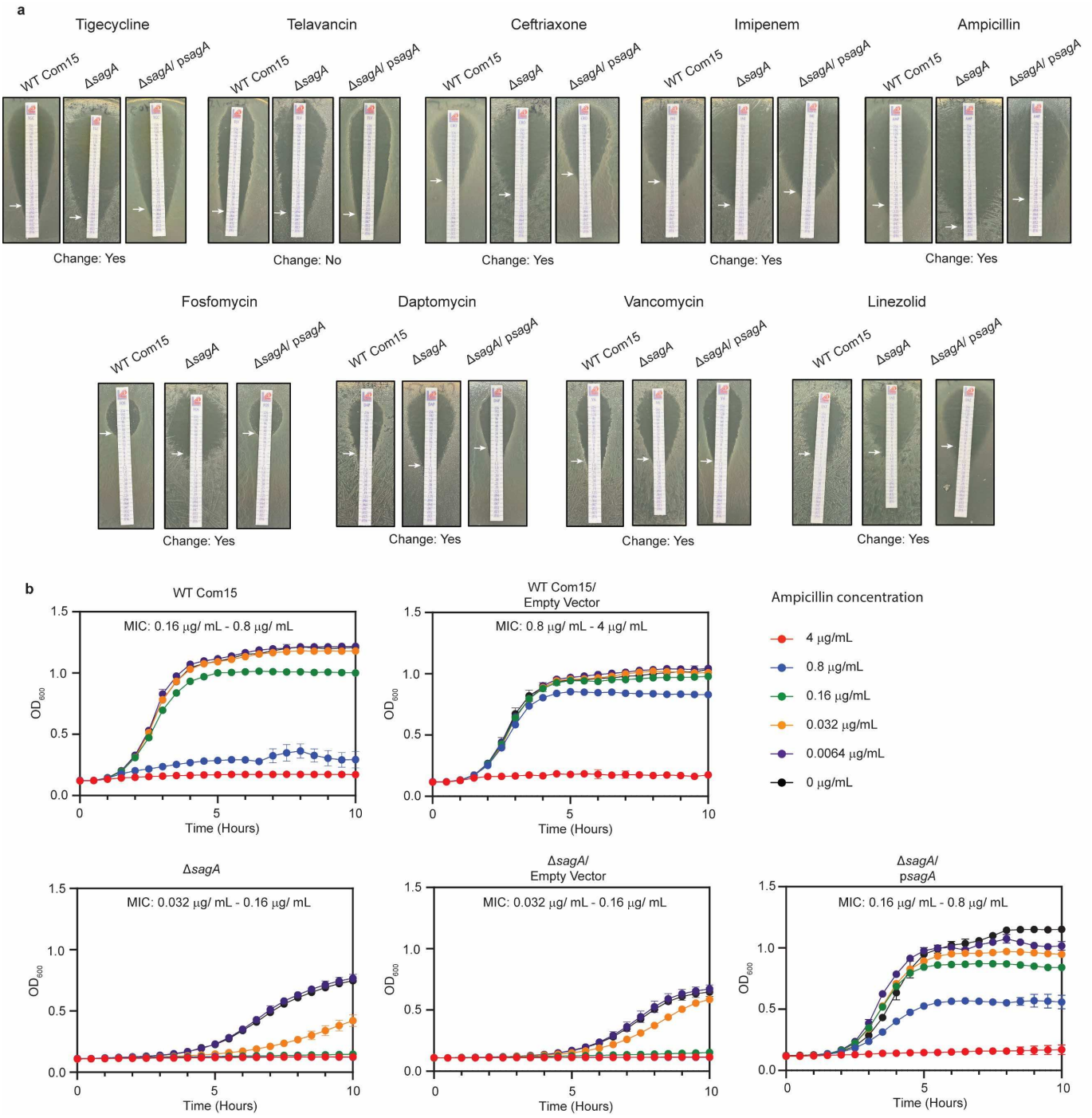

Extended Data Figure 2. Antibiotic sensitivity of Δ*sagA*. a, Approximate MIC determinations via antibiotic test strips for *E. faecium* WT Com15, Δ*sagA* and Δ*sagA*/ p*sagA*. **b,** Liquid culture MIC determination for ampicillin.

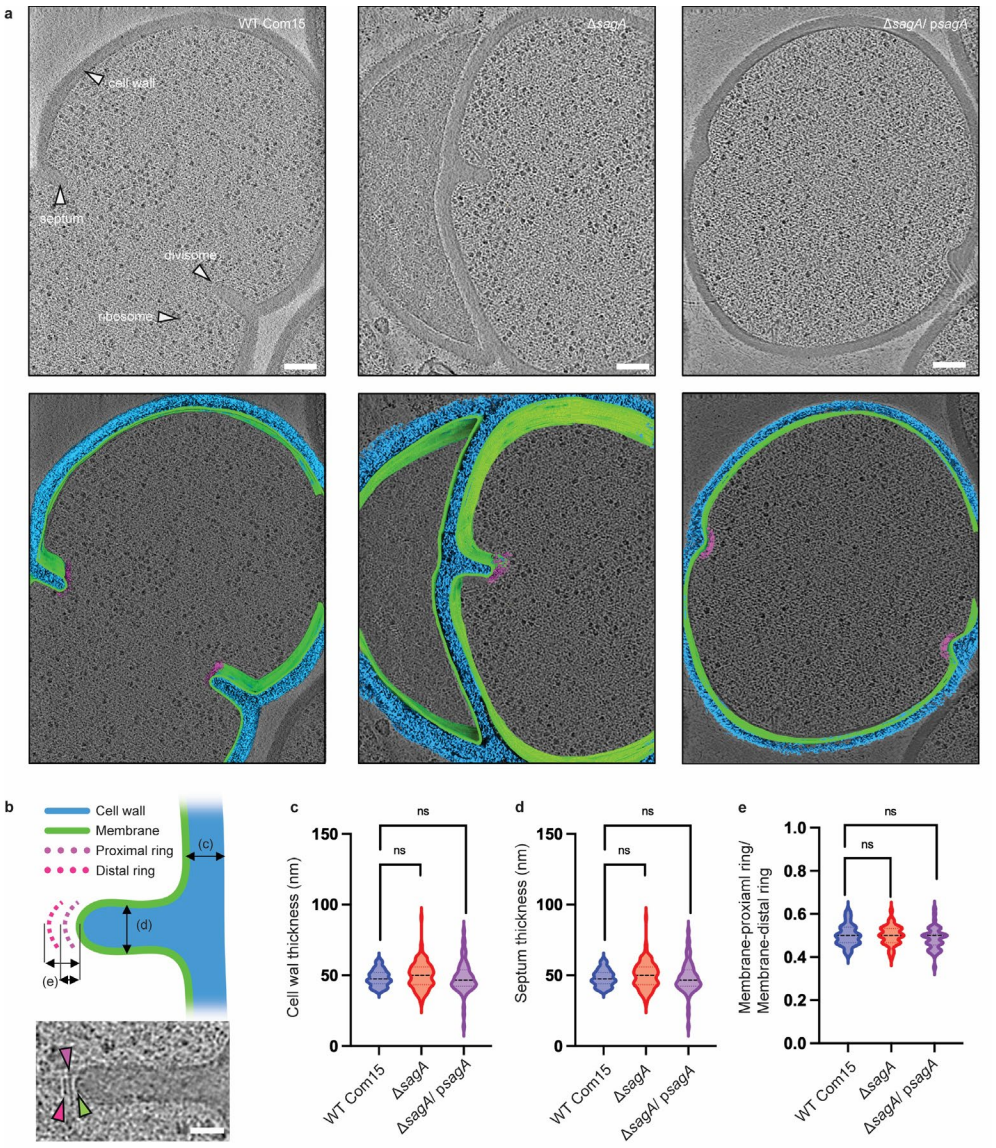

Extended Data Figure 3. *E. faecium* Δ*sagA* exhibits no defects in cell wall and septum thickness. a, Representative cryo-ET images of *E. faecium* WT Com15, Δ*sagA*, and Δ*sagA*/p*sagA* are shown in the top row. The cell wall, septum, divisome, and ribosome are indicated by white arrows. 3D segmentations are shown in the bottom row. The cell wall is annotated in blue, the membrane in green, and the divisome in magenta. Scale bar = 100 nm. **b**, The upper panel shows a diagram illustrating how measurements are collected. In the lower panel, a representative cryo-ET image of the septum is shown. Scale bar = 50 nm. **c**, Comparison of cell wall thickness. The violin plot displays the distribution of cell wall thickness, with *E. faecium* WT Com15 WT (n=66) shown in blue, *ΔsagA* (n=96) shown in red, and *ΔsagA*/ p*sagA* (n=69) shown in magenta. Black dotted lines represent median (*E. faecium* WT Com15 WT: 47.48nm, *ΔsagA*: 50.11nm, *ΔsagA*/ p*sagA*: 46.42nm) while the colored dotted lines represent quartiles. Welch's *t* test was used to calculate statistical significance. ns, $P \geq 0.05$. **d**, Comparison of septum thickness. The violin plot displays the distribution of septum thickness, with *E. faecium* WT Com15 WT (n=26) shown in blue, *ΔsagA* (n=62) shown in red, and *ΔsagA*/p*sagA* (n=16) shown in magenta. Black dotted lines represent median (*E. faecium* WT Com15: 54.33nm, *ΔsagA*: 54.86nm, *ΔsagA*/ p*sagA*: 57.50nm) while the colored dotted lines represent quartiles. Welch's *t* test was used to calculate statistical significance. ns, $P \geq 0.05$. (**e**) Comparison of divisome architecture. To assess potential alterations in the divisome architecture, the distance between the apical end of the septum and the membrane-proximal ring was divided by the distance between the apical end of the septum and the membrane-distal ring. The violin plot displays the distribution of the ratios, with *E. faecium* WT Com15 WT (n=31) shown in blue, *ΔsagA* (n=40) shown in red, and *ΔsagA*/ p*sagA* (n=42) shown in magenta. Black dotted lines represent median (*E. faecium* WT Com15: 0.5, *ΔsagA*: 0.5, *ΔsagA*/ p*sagA*: 0.5) while the colored dotted lines represent quartiles. Welch's *t* test was used to calculate statistical significance. ns, $P \geq 0.05$.

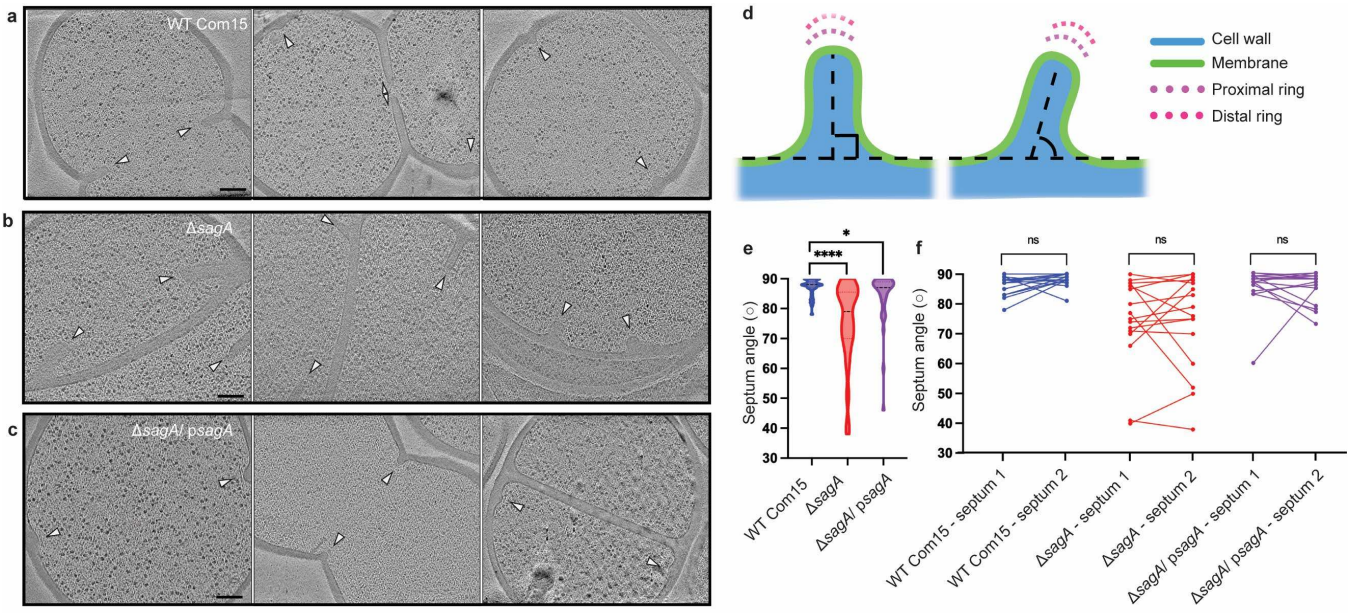

Figure 2. **Deletion of *sagA* changes the angle of growing septum. a-c**, Representative tomographic slices of three *E. faecium* strains: *E. faecium* WT Com15 (**a**), Δ*sagA* (**b**), and Δ*sagA*/p*sagA* (**c**). Cell division septa are indicated by white arrows. Scale bar = 100 nm. **d**, A diagram indicating how septum angle measurements were collected. Acute angles are recorded for further analysis. **e**, Comparison of septum angle. The violin plot displays the distribution of septum angle, with *E. faecium* WT Com15 WT (n=40) shown in blue, *ΔsagA* (n=49) shown in red, and *ΔsagA*/ p*sagA* (n=37) shown in magenta. Black dotted lines represent median (*E. faecium* wt: 88°, *ΔsagA*: 79°, *ΔsagA*/p*sagA*: 87°) while the colored dotted lines represent quartiles. Welch's *t* test was used to calculate statistical significance. *, $P < 0.05$; ****, $P < 0.0001$. **f**, Pairwise comparison of septum angle in opposing septa. The paired plot displays the distribution of septum angle, with *E. faecium* WT Com15 WT (n=18) shown in blue, *ΔsagA* (n=16) shown in red, and *ΔsagA*/ p*sagA* (n=16) shown in magenta. Two septum angles from opposing septa are linked with straight lines. Paired *t* test was used to calculate statistical significance. ns, $P \geq 0.05$.

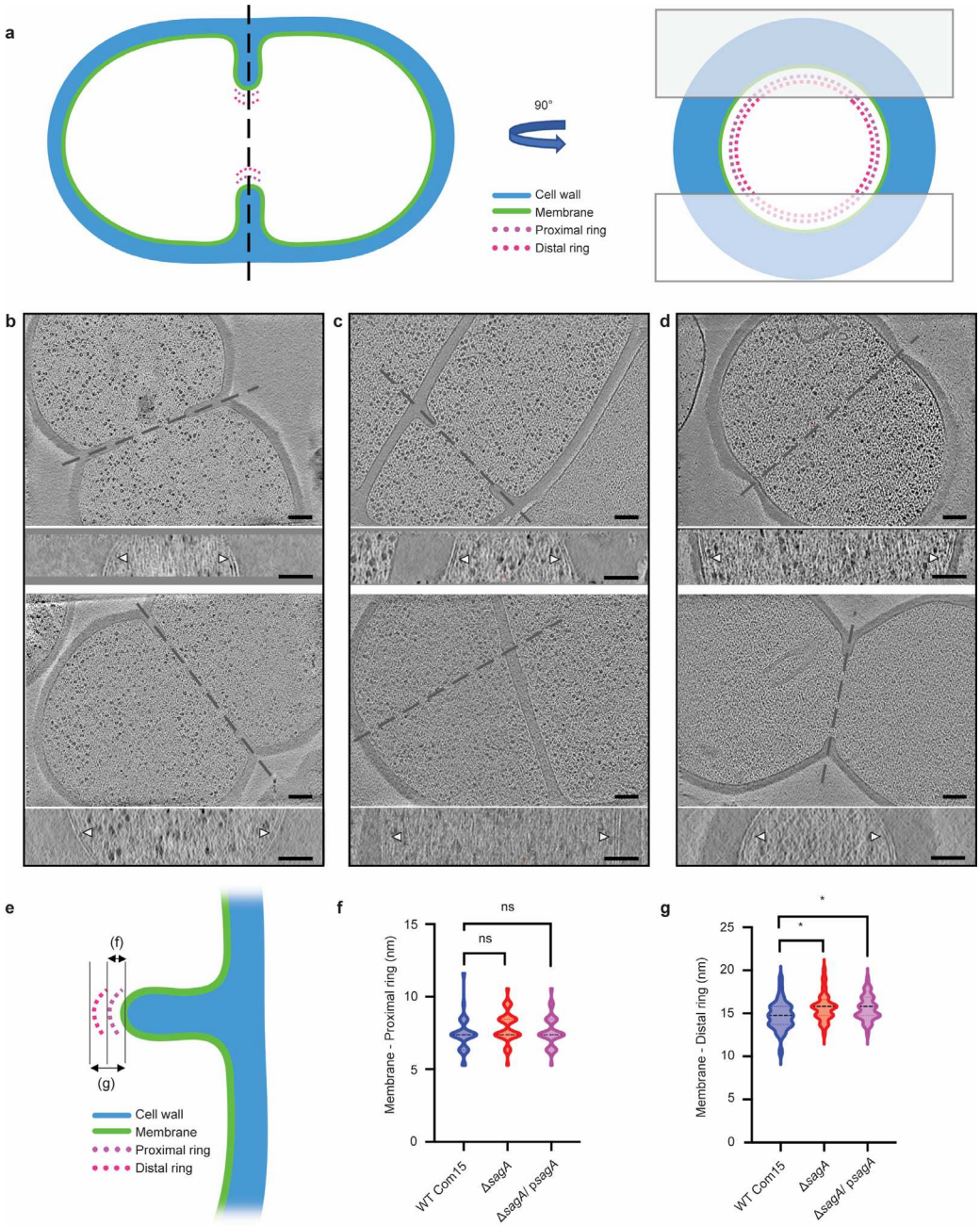

Extended Data Figure 4. Deletion of *sagA* alters the position of cell division. a, Cartoon model depicting cell division site in the xy coordinate plane (left) and xz coordinate plane (right). The two boxes shown in right represent the cryo-focused ion beam (cryo-FIB) milling patterns used to generate thin sections of *E. faecium* for subsequent cryo-electron tomography (cryo-ET) imaging. **b-d**, Representative tomographic slices of three *E. faecium* strains: *E. faecium* WT Com15 (**b**), Δ*sagA* (**c**), and Δ*sagA*/ p*sagA* (**d**). The upper panels show view of dividing cells in the xy coordinate plane and, while the corresponding bottom panels show the divisome complex (annotated with white arrows) at the highlighted areas in the corresponding upper panels in the xz coordinate plane, obtained by rotating the cell 90° along the highlighted axis. Scale bar = 100 nm. **e**, A diagram indicating how measurements were collected. **f**, Comparison of membrane to proximal ring distance. The violin plot displays the distribution of distance between the apical end of septum membrane to the proximal ring, with *E. faecium* WT Com15 (n=31) shown in blue, *ΔsagA* (n=40) shown in red, and *ΔsagA*/ p*sagA* (n=42) shown in magenta. Black dotted lines represent median (*E. faecium* WT Com15: 7.39nm, *ΔsagA*: 7.39nm, *ΔsagA*/ p*sagA*: 7.39nm) while the colored dotted lines represent quartiles. Welch's *t* test was used to calculate statistical significance. ns, $P \geq 0.05$. **g**, Comparison of membrane to distal ring distance. The violin plot displays the distribution of distance between the apical end of septum membrane to the distal ring, with *E. faecium* WT Com15 (n=31) shown in blue, *ΔsagA* (n=40) shown in red, and *ΔsagA*/ p*sagA* (n=42) shown in magenta. Black dotted lines represent median (*E. faecium* WT Com15: 14.77nm, *ΔsagA*: 15.83nm, *ΔsagA*/ p*sagA*: 15.83nm) while the colored dotted lines represent quartiles. Welch's *t* test was used to calculate statistical significance. *, $P < 0.05$.

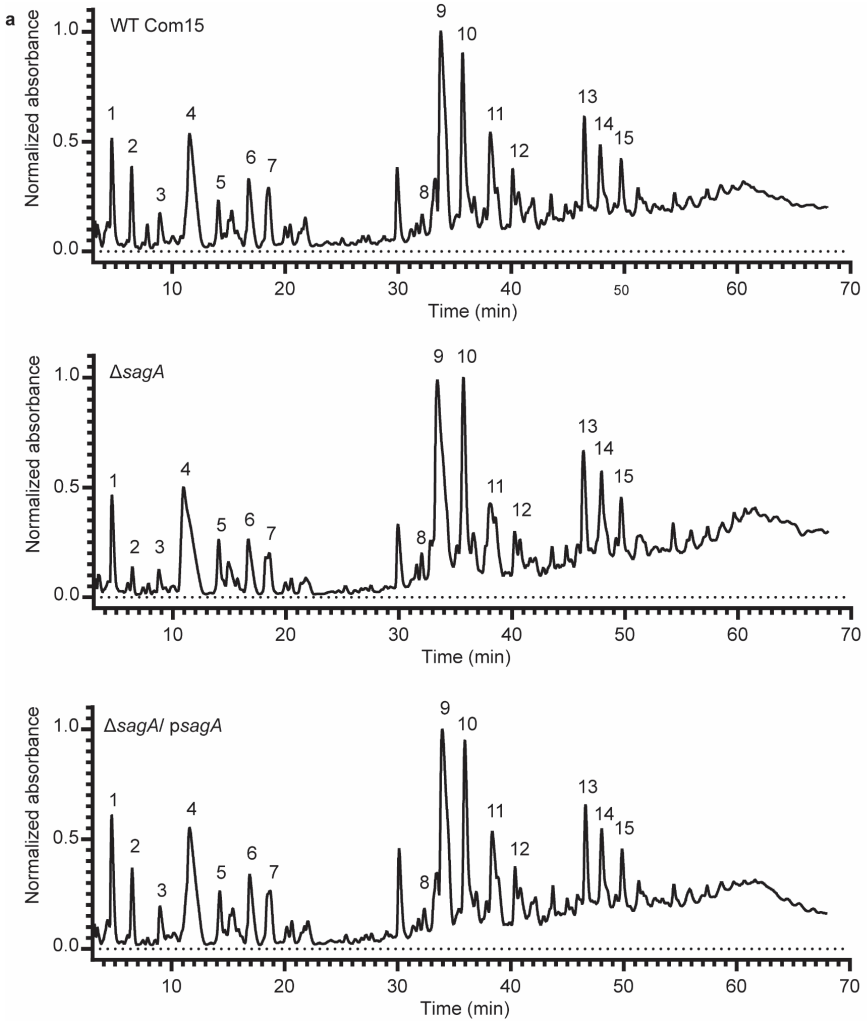

b

Peak #[a]	Proposed structure[b]
1	GM-tri
2	GMDP
3	GM-tetra
4	GM-tri (Asn)[c]
5	GM-tri (Asp)[c]
6	GM-tetra (Asn)
7	GM-tetra (Asx)
8	2GM-tri (Asx) - tetra
9	2GM-tri (Asn) - tetra (Asn)[c]
10	2GM-tri (Asx) - tetra (Asx)[c]
11	2GM-tetra (Asn) - tetra (Asn)[c]
12	2GM-tetra (Asp) - tetra (Asp)[c]
13	3GM-tetra (Asx) - tetra (Asx) - tri (Asx)[c]
14	3GM-tetra (Asx) - tetra (Asx) - tri (Asx)[c]
15	3GM-tetra (Asx) - tetra (Asx) - tetra (Asx)

Extended Data Figure 5. Peptidoglycan profile of *E. faecium* Δ*sagA* by LC-MS. a, LC-MS analysis of peptidoglycan isolated from *E. faecium* WT Com15 (top), Δ *sagA* (middle), and Δ *sagA*/p*sagA* (bottom). Numbers correspond to each muropeptide annotated in the table (**b**). **b,** Composition of muropeptides from *E. faecium*. [a.] Peak numbers refer to (**a**). [b.]GM, disaccharide (GlcNAc-MurNAc); 2GM, disaccharide-disaccharide (GlcNAc-MurNAc-GlcNAc-MurNAc); 3GM, disaccharide-disaccharide-disaccharide (GlcNAc-MurNAc-GlcNAc-MurNAc-GlcNAc-MurNAc); GM-Tri, disaccharide tripeptide (L-Ala-D-iGln-L-Lys); GM-Tetra, disaccharide tetrapeptide (L-Ala-D-iGln-L-Lys-D-Ala); GM-Penta, disaccharide pentapeptide (L-Ala-D-iGln-L-Lys-D-Ala -D-Ala). [c.] The assignment of the amide and the hydroxyl functions to either peptide stem is arbitrary.

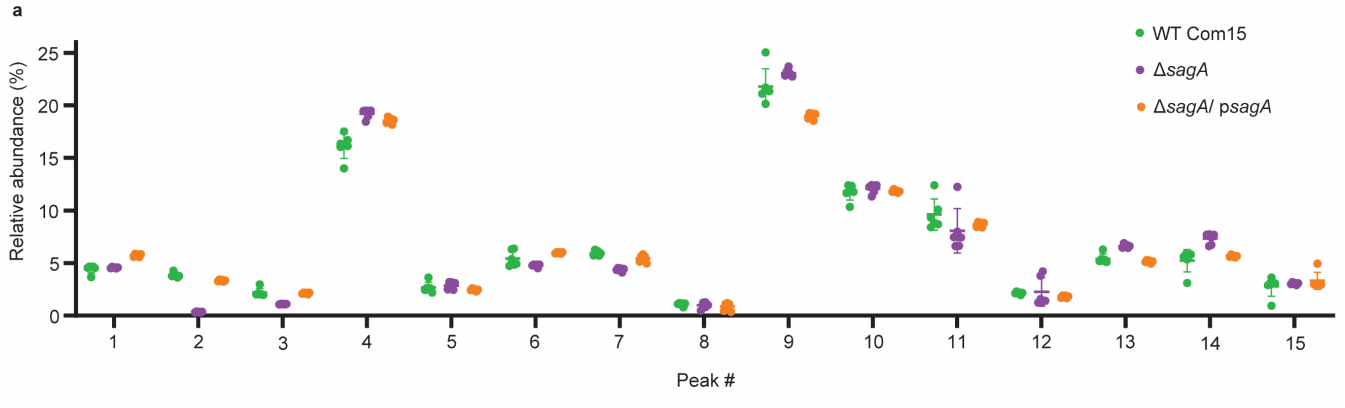

b

Peak #[a]	Proposed structure[b]
1	GM-tri
2	GMDP
3	GM-tetra
4	GM-tri (Asn)[c]
5	GM-tri (Asp)[c]
6	GM-tetra (Asn)
7	GM-tetra (Asx)
8	2GM-tri (Asx) - tetra
9	2GM-tri (Asn) - tetra (Asn)[c]
10	2GM-tri (Asx) - tetra (Asx)[c]
11	2GM-tetra (Asn) - tetra (Asn)[c]
12	2GM-tetra (Asp) - tetra (Asp)[c]
13	3GM-tetra (Asx) - tetra (Asx) - tri (Asx)[c]
14	3GM-tetra (Asx) - tetra (Asx) - tri (Asx)[c]
15	3GM-tetra (Asx) - tetra (Asx) - tetra (Asx)

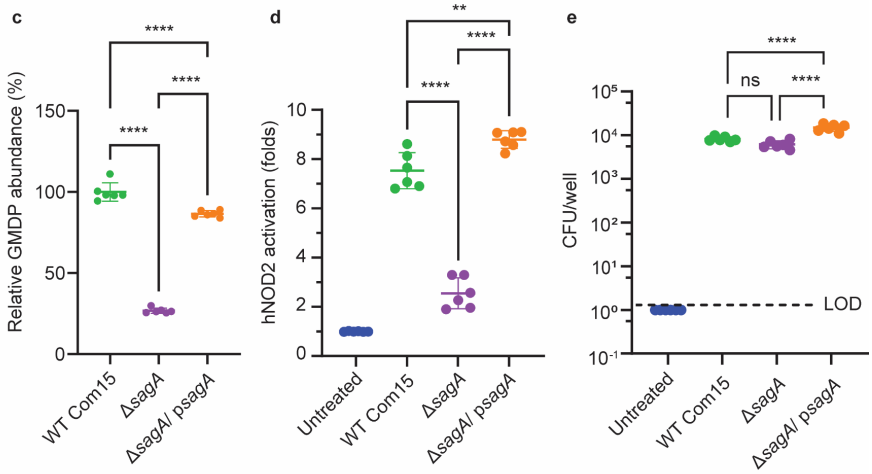

Figure 3. Peptidoglycan profile and NOD2 activation of *E. faecium* ΔsagA. **a**, Relative abundance of muropeptides isolated from *E. faecium* strains (n=6). Data are presented as mean value ± standard deviation and analyzed with one-way ANOVA and Tukey's multiple comparison post hoc test. *p≤0.05; **p≤0.01; ***p≤0.005; ****p≤0.001. Numbers correspond different muropeptides from LC-MS analysis listed in legend. **b**, Composition of muropeptides from *E. faecium*. [a.] Peak numbers refer to (**a**). [b.]GM, disaccharide (GlcNAc-MurNAc); 2GM, disaccharide-disaccharide (GlcNAc-MurNAc-GlcNAc-MurNAc); 3GM, disaccharide-disaccharide-disaccharide (GlcNAc-MurNAc-GlcNAc-MurNAc-GlcNAc-MurNAc); GM-Tri, disaccharide tripeptide (L-Ala-D-iGln-L-Lys); GM-Tetra, disaccharide tetrapeptide (L-Ala-D-iGln-L-Lys-D-Ala); GM-Penta, disaccharide pentapeptide (L-Ala-D-iGln-L-Lys-D-Ala -D-Ala). [c.] The assignment of the amide and the hydroxyl functions to either peptide stem is arbitrary. **c,** Relative abundance of GMDP from LC-MS chromatograms (n=6). **d**, NF-κB responses of HEK-Blue™ hNOD2 cells to live *E. faecium* strains (MOI=1). **e**, Colony forming units (CFU) of *E. faecium* strains (MOI = 1) internalized in HEK-Blue™ hNOD2 cells (n=6). Dashed line indicates Limit of Detection (LOD). Data are presented as mean value ± standard deviation and analyzed with one-way ANOVA and Tukey's multiple comparison post hoc test. *p≤0.05; **p≤0.01; ***p≤0.005; ****p≤0.001; ns, not significant.

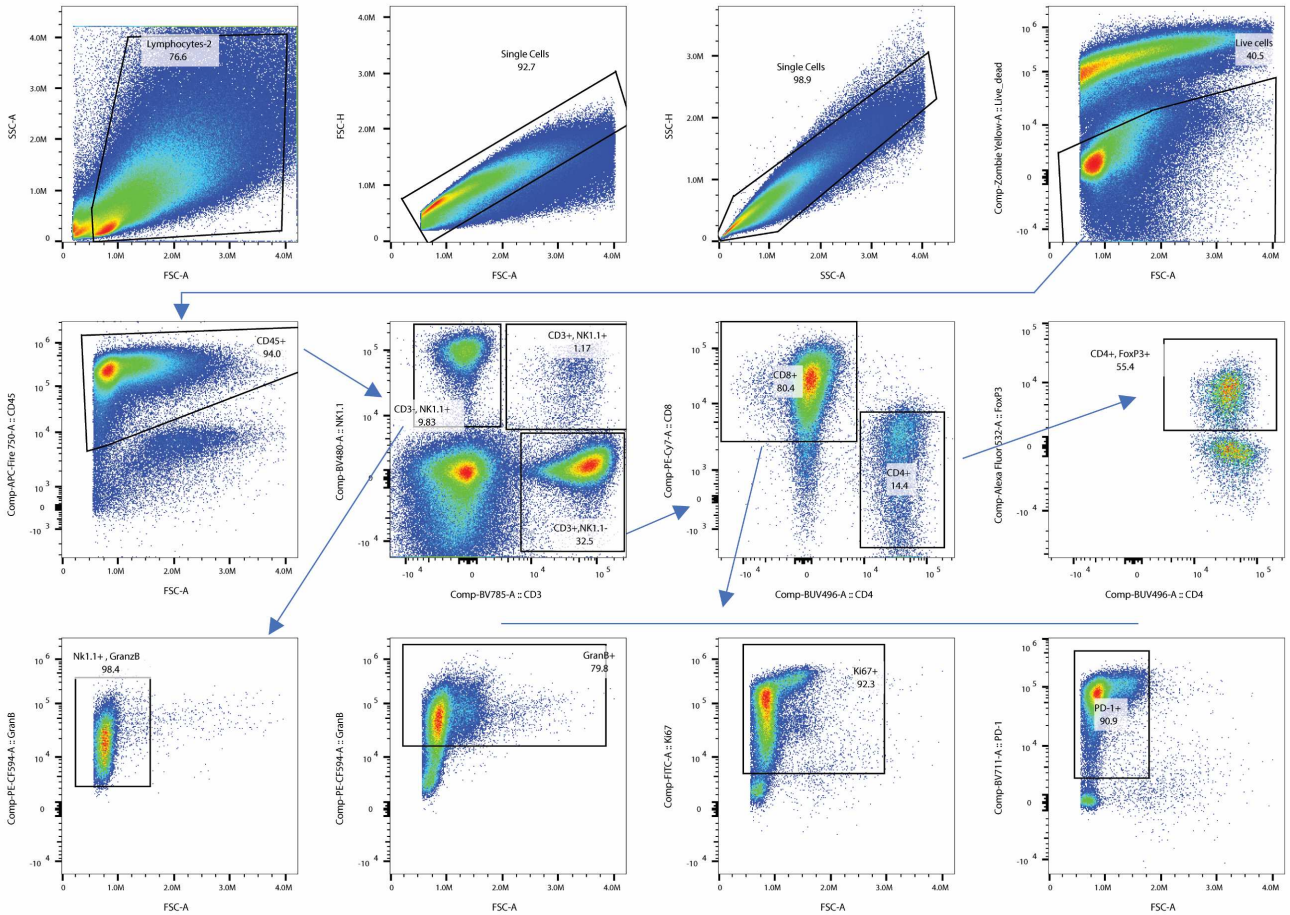

Extended Data Figure 6. Gating strategy used for flow cytometry analysis of TILs.

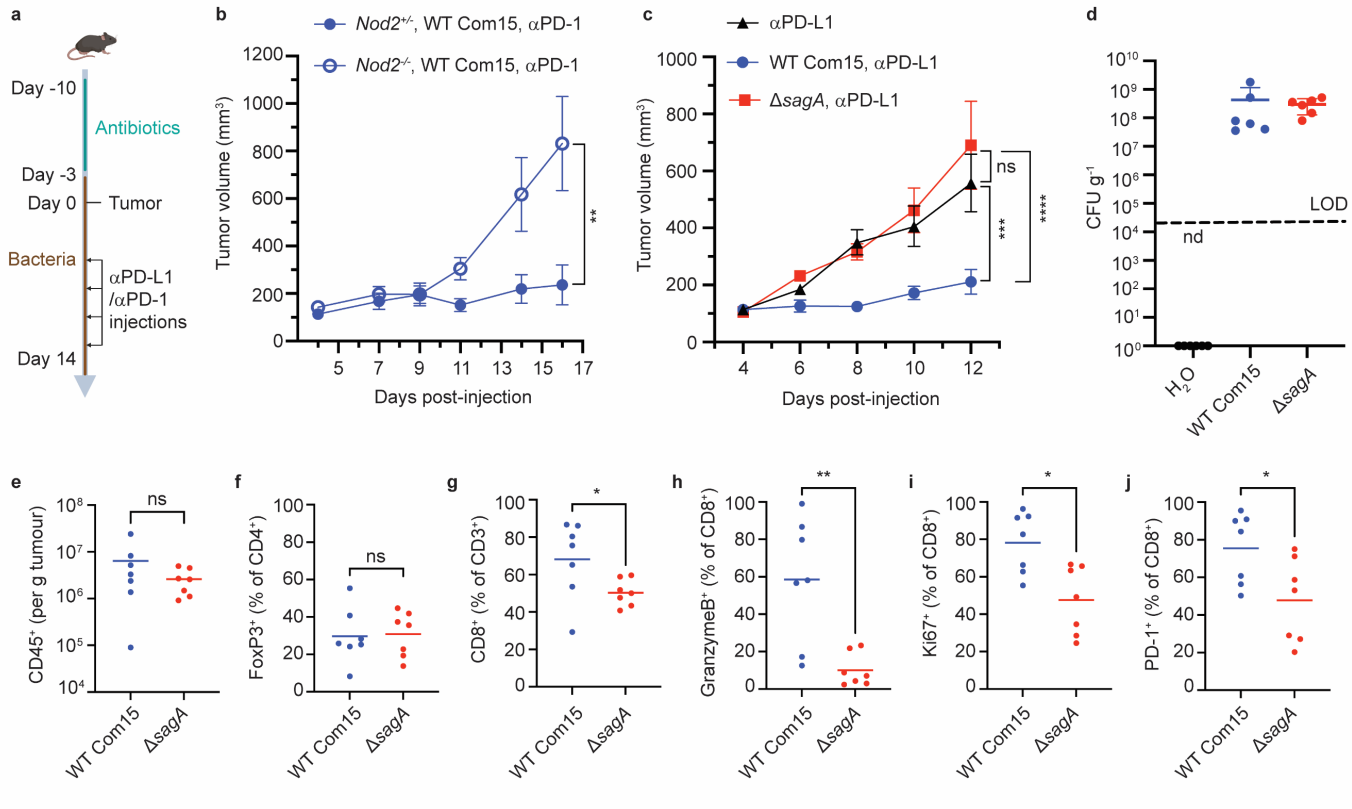

Figure 4. Immune checkpoint inhibitor antitumor activity and tumor immune profile of *E. faecium* Δ*sagA* colonized mice. a, Schematic of tumor growth experiment: mice were provided water containing antibiotics for 1 week and started to drink bacteria three days before tumor implantation. Once the tumor reaches ~100 mm^3, the measurement starts and two days after treated with anti-PD-1 for MC38 or anti-PD-L1 for B16F10 every other day. **B**, MC-38 tumor growth in *Nod2*$^{+/-}$ or *Nod2*$^{-/-}$ mice that colonized with *E. faecium* WT Com15 and treated with anti-PD-1 starting at day 7. N=10 for *Nod2*$^{+/-}$ mice, n=6 for *Nod2*$^{-/-}$ mice. **c**, B16F10 tumor growth in C57BL/6 mice that colonized without bacteria (water) or with *E. faecium* WT Com15 *or* Δ*sagA* and treated with anti-PD-L1 starting at day 6. N=7-8 mice per group. **d**, Fecal CFU analysis of *E. faecium* on HiCrome plate from I at day 6. N=6 per group. Each dot represents one mouse. The line indicates the limit of detection, LOD (4000 CFU g^{-1}). Nd, not detected. Data represent means ± 95% confidence interval. **E-j**, Quantification of tumor infiltrating CD45$^+$ cells I, FoxP3$^+$ cells (**f**), CD3$^+$ CD8$^+$ cells (**g**), GranzymeB$^+$ CD8$^+$ T cells (**h**), Ki67$^+$ CD8$^+$ T cells (**i**) and PD-1$^+$ CD8$^+$ T cells (**j**). For **f, h-j**, fluorescence minus one (FMO) control was used to define gates. N=7 mice per group. Data for **b** and **c** represent mean ± SEM. And were analyzed using a mixed effects model with Tukey's multiple comparisons post hoc test. Data for **e-j** represent mean ± SEM. And were analyzed by the Mann-Whitney U (one-tail) test. *P < 0.05, **P < 0.01, ***P < 0.001, ****P < 0.0001; ns, not significant.

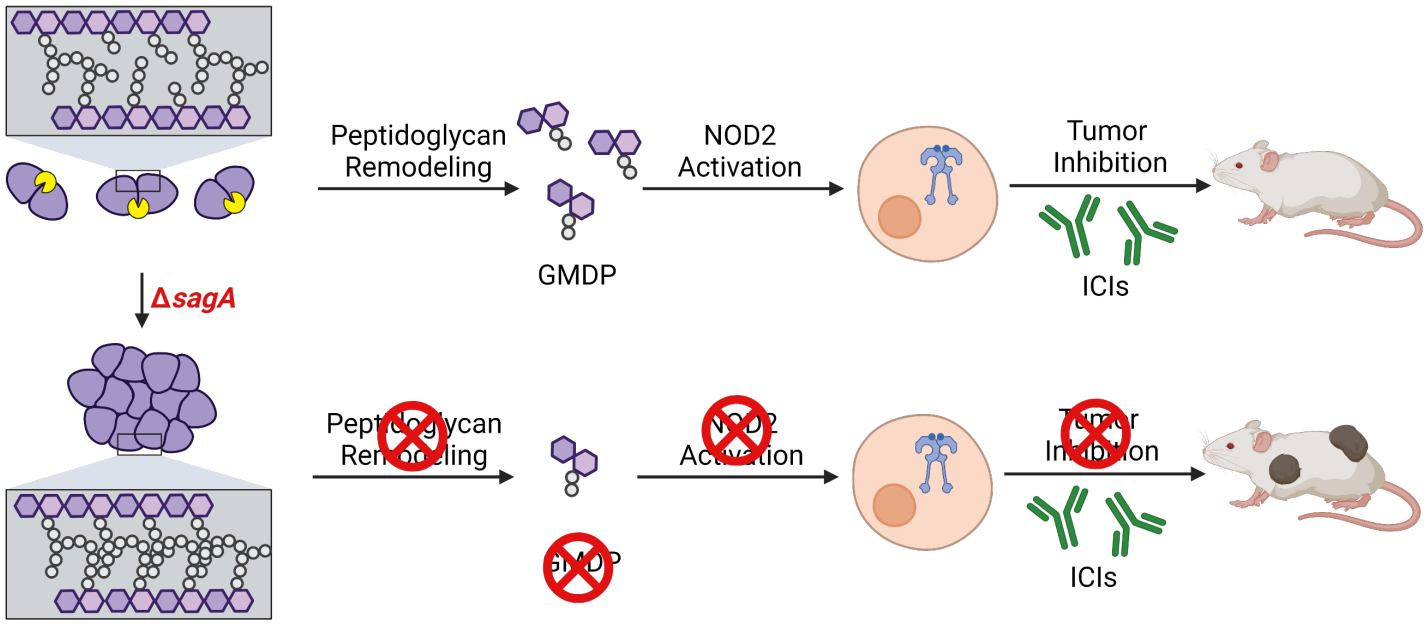

Extended Data Figure 7. Summary of SagA function in *E. faecium* and impact on host immunity during ICI cancer therapy. Deletion of *sagA* impairs peptidoglycan remodeling and cell separation in *E. faecium* and limits the activation of NOD2 in mammalian cells to promote immune checkpoint inhibitor cancer therapy in mouse models. Created with BioRender.com.

Extended Data Table 1. Mutations detected in Δ*sagA E. faecium* Com15 strain.

Genomic locus	BioCyc annotation	Type of mutation	Notes
EFWG_00994	Mannosyl-glycoprotein endo-beta-n-acetylglucosaminidase	missense (L200F)	L200 is a conserved residue among GH73 family proteins
EFWG_01683	50S ribosomal protein L4	missense (E16K)	
EFWG_02413	aquaporin family protein	missense (A45T)	
EFWG_02113	folate family ECF transporter S component	promoter (-10 site)	promoter identified with BPROM
EFWG_01149	LacI family transcriptional regulator	silent (L270L)	
between EFWG_01661 and EFWG_01662	N/A	intergenic	
between EFWG_02410 and EFWG_02411	N/A	intergenic	
upstream of EFWG_02718	N/A	intergenic	
immediately downstream of EFWG_04048	N/A	intergenic	
EFWG_02083	collagen-binding protein	insertion/ duplication	There is an apparent duplication of a 78bp fragment, however it is adjacent to a stretch of undefined sequence. Thus, this mutation may not truly be present, and may just be a result of incomplete sequencing.
EFWG_11565	pseudogene	3x silent (A451A, A453A, A457A) and insertion/ frameshift	EFWG_RS11565 is annotated in BioCyc as a pseudogene because of a premature stop codon that splits the gene into two ORFs. The frameshift mutation in Δ*sagA* returns the gene to a single ORF.

Extended Data Table 2: *E. faecium* strains used in this study.

Strain	Description	Source
E. faecium	*E. faecium* Com15	lab stock
VC109	Com15 harboring the pRecT plasmid	Chen V et al.[20]
SK057	Δ*sagA*	this work
SK080	Δ*sagA*/ empty vector	this work
SK081	Δ*sagA*/ p*sagA*^{C431A}	this work
SK106	*E. faecium* wt/ empty vector	this work
SK109	Δ*sagA*/ p*sagA(v2)*	this work

Extended Data Table 3: Plasmids used in this study.

Plasmid	Description	Source
pET21a	backbone used for assembling deletion constructs	lab stock
pAM401	backbone for plasmids to be transformed into *E. faecium*	lab stock
pRecT	recombinase-harboring plasmid used to facilitate *E. faecium* deletions	Chen V et al.[20]
p*sagA*	pAM401-based plasmid that contains *sagA* under the control of its native promoter	Espinosa J et al.[21]
pSK060	modified p*sagA* that swaps a cm^R cassette for an erm^R cassette (referred to in the main text, and in the plasmids below as "p*sagA*")	this work
pSK069	pAM401 with erm^R empty vector	this work
pSK071	p*sagA*^{C443A}	this work
pSK104	p*sagA(v2)* (referred to as "p*sagA*" in the main text)	this work

Extended Data Table 4: Primers used in this study for generating complementation plasmids and empty vector.

Deletion	PCR Fragment Generated	Primer Name	Sequence (5' to 3')
SagA	homology arm 1	oSK025	TTTTGTTTAACTTTAAGAAGGAGATATACAA ACTCCATGCATTAGTGGTGAC
		oSK026	ATCTATCTTGAGTTTCAATCTATTTTTTTTTC TTCATTCCTCCGACTGGC
	cm^R cassette	oSK008	TAAATTTAACGATCACTCAAAAAATTATAAA AGCCAGTC
		oSK009	AAAAAAAATAGATTGAAACTCAAGATAGATA TGTTATTG
	homology arm 2	oSK027	TTTATAATTTTTTGAGTGATCGTTAAATTTAG AATGATTAATCAAAAAGAGTTAGTCCAG
		oSK028	GCCGGATCTCAGTGGTGGTGGTGGTGGTG CGTAAGGAAAAAATGGAATGGCAG
	complete deletion construct	oSK041	AACTCCATGCATTAGTGGTGAC
		oSK042	GTAAGGAAAAAATGGAATGGCAG
	verification of deletion	oSK368	CTTTCTAACTATGAACTTCATGGC
		oSK369	TCCAGTACGGGTATCTTC

Purpose	Fragment	Primer Name	Sequence (5' to 3')
generating pSK060 by swapping cm^R for erm^R in p*sagA* using two-fragment Gibson assembly	p*sagA* backbone	oSK406	TTACTTCCAAAACCTAAATTCACGTT G
		oSK407	TAAATTATTTAATAAGTAATTTTTAGA TTTTGAAAGTGAATTTAATTTTATACA CGTAAG
	erm^R cassette	oSK408	GATTTTTGGCAACGTGAATTTAGGTT TTGGAAGTAACATGTTCATATTTATC AGAGCTCG
		oSK409	TTCAAAATCTAAAAATTACTTATTAAA TAATTTATAGCTATTGAAAAGAGATA AGAATTG
generating pSK069 by removing *sagA* from p*sagA* using Q5-SDM (NEB)	linearized pSK069 plasmid	oSK475	GTCGACCGATGCCCTTGAGAGC
		oSK476	AGGATCCACAGGACGGGTGTG
generating pSK104 using two-fragment Gibson assembly	pSK060 backbone	oSK562	TATGTTTGGGGCGGTAAAGATC
		oSK563	AGTGTAGGCCCTAAGAACCTTG
	alternate *sagA* sequence	oSK564	TTTTATTACAAGGTTCTTAGGGCCTA CACT
		oSK565	TCCACTTGGATCTTTACCGCCCCAA ACATA

Mutagenesis of the *sagA* gene in p*sagA* was accomplished using the Q5 Site-Directed Mutagenesis kit (NEB), according to the manufacturer's instructions. The primers used for mutagenesis are reported in **Extended Data Table 5**.

Extended Data Table 5: Primers used in this study for SagA mutagenesis.

Mutation	Primer Name	Sequence (5' to 3')
C431A	oSK479	TCCAAGTGGATTTGACGCCTCAGGATTCACACGCTATG TTTACTTGCAAGTAACTGG
	oSK480	TCTTTACCGCCCCAAACATAAGGAGTACCAATATATTTG

Extended Data Table 6: Masses of peptidoglycan fragments were detected with MSD API-ES.

Peak[a]	RT (min)	calculated $[M+H]^+$	observed $[M+H]^+$	Proposed structure[b]
1	4.96	826.4	828.6	GM-tri
2	6.46	698.2	698.4	GMDP
3	9.15	897.4	897.6	GM-tetra
4	11.85	940.4	940.6	GM-tri (Asn)[c]
5	14.26	941.4	941.4	GM-tri (Asp)[c]
6	16.95	1011.5	1011.6	GM-tetra (Asn)
7	18.70	1082.5	1082.6	GM-penta (Asx)
8	32.11	1819.9	1819.4	2GM-tri (Asx) - tetra
9	33.77	1933.9	1934.4	2GM-tri (Asn) - tetra (Asn)[c]
10	35.69	1934.9	1935.2	2GM-tri (Asx) - tetra (Asx)[c]
11	38.15	2004.9	2005.2	2GM-tetra (Asn) - tetra (Asn)[c]
12	40.13	2006.9	2007.2	2GM-tetra (Asp) - tetra (Asp)[c]
13	46.52	2928.4	2929.2	3GM-tetra (Asx) - tetra (Asx) - tri (Asx)[c]
14	47.94	2929.4	2929.8	3GM-tetra (Asx) - tetra (Asx) - tri (Asx)[c]
15	51.29	3000.4	3000.6	3GM-tetra (Asx) - tetra (Asx) - tetra (Asx)

[a.] Peak numbers refer to Extended Data Figure 5a.
[b.] GM, disaccharide (GlcNAc-MurNAc); 2GM, disaccharide-disaccharide (GlcNAc-MurNAc-GlcNAc-MurNAc); 3GM, disaccharide-disaccharide-disaccharide (GlcNAc-MurNAc-GlcNAc-MurNAc- GlcNAc-MurNAc); GM-Tri, disaccharide tripeptide (L-Ala-D-iGln-L-Lys); GM-Tetra, disaccharide tetrapeptide (L-Ala-D-iGln-L-Lys-D-Ala); GM-Penta, disaccharide pentapeptide (L-Ala-D-iGln-L-Lys-D-Ala -D-Ala).
[c.] The assignment of the amide and the hydroxyl functions to either peptide stem is arbitrary.